Spectrochimica Acta Part B 150 (2018) 99–104

Contents lists available at ScienceDirect

Spectrochimica Acta Part B

journal homepage: www.elsevier.com/locate/sab

Radium ionization scheme development: The first observed autoionizing states and optical pumping effects in the hot cavity environment

T. Day Goodacre[a,b,*,1], J. Billowes[b], C.L. Binnersley[b], M.L. Bissell[b], K. Chrysalidis[a,c], T.E. Cocolios[d], R.P. de Groote[d], G.J. Farooq-Smith[d], D.V. Fedorov[e], V.N. Fedosseev[a], K.T. Flanagan[b,f], S. Franchoo[g], R.F. Garcia Ruiz[b], W. Gins[d], R. Heinke[c], Á. Koszorús[d], K.M. Lynch[a], B.A. Marsh[a], P.L. Molkanov[e], P. Naubereit[c], G. Neyens[a], C.M. Ricketts[b], S. Rothe[a], C. Seiffert[a], M.D. Seliverstov[e], H.H. Stroke[h], D. Studer[c], A.R. Vernon[b], S.G. Wilkins[b], K.D.A. Wendt[c], X.F. Yang[d]

[a] EN Department, CERN, Geneva CH-1211, Switzerland
[b] School of Physics and Astronomy, The University of Manchester, Manchester M13 9PL, United Kingdom
[c] Institut für Physik, Johannes Gutenberg-Universität, Mainz D-55099, Germany
[d] Instituut voor Kern- en Stralingsfysica, KU Leuven, Leuven B-3001, Belgium
[e] Petersburg Nuclear Physics Institute, Gatchina 188350, Russia
[f] The Photon Science Institute, The University of Manchester, Manchester, M13 9PL, United Kingdom
[g] Institut de Physique Nucléaire d'Orsay, Orsay F-91406, France
[h] Department of Physics, New York University, New York, NY 10003, USA

ARTICLE INFO

Keywords:
RILIS
ISOLDE
Radium
Autoionizing states
Laser ionization

ABSTRACT

This paper reports on resonance ionization scheme development for the production of exotic radium ion beams with the Resonance Ionization Laser Ion Source (RILIS) of the CERN-ISOLDE radioactive ion beam facility. During the study, autoionizing states of atomic radium were observed for the first time. Three ionization schemes were identified, originating from the $7s^2\ ^1S_0$ atomic ground state. The optimal of the identified ionization schemes involves five atomic transitions, four of which are induced by three resonantly tuned lasers. This is the first hot cavity RILIS ionization scheme to employ optical pumping effects. The details of the spectroscopic studies are described and the new ionization schemes are summarized.

1. Introduction

The principal ion source of the ISOLDE radioactive ion beam facility [1] based at CERN is the Resonance Ionization Laser Ion Source (RILIS) [2,3]. The RILIS uses tunable lasers to excite valence electrons by targeting sequential atomic resonances before a final ionizing transition, typically either to an autoionizing state or non-resonant excitation to the ionization continuum. The selectivity of the ionization mechanism is a result of the element unique nature of atomic energy levels. However, it also follows that an "ionization scheme" of sequential resonances has to be tested and developed for each element that the RILIS is applied for. Excitation to an autoionizing state is typically the preferred method of ionization in resonance ionization spectroscopy (RIS) [4]. This is because the cross-section for a resonant transition can be orders of magnitude greater than for non-resonant excitation to the ionization continuum.

Despite having no stable isotopes, optical spectroscopy of atomic radium has been ongoing for > 100 years [5]. However, prior to this work no autoionizing states had been identified. Here we present the results of ionization scheme development for atomic radium including three new ionization schemes, the first identification of autoionizing states of atomic radium and the first harnessing of optical pumping effects within a hot cavity RILIS ionization scheme.

1.1. Radioactive ion beam production at ISOLDE

ISOLDE is an ISOL type [6] radioactive ion beam facility. A pulsed 2 μA average power "driver beam" of 1.4 GeV protons from the CERN

* Corresponding author at: Accelerator Science Division, TRIUMF, Vancouver BC V6T 2A3, Canada.
E-mail address: tdaygoodacre@triumf.ca (T. Day Goodacre).
[1] Present address: Accelerator Science Division, TRIUMF, Vancouver BC V6T 2A3, Canada.

https://doi.org/10.1016/j.sab.2018.10.002
Received 13 June 2018; Received in revised form 28 September 2018; Accepted 1 October 2018
Available online 09 October 2018

proton synchrotron booster (PSB) is impinged upon a target to generate radiogenic reaction products. These are then stopped and thermalized within the target material. During operation, the target is typically heated to ≈2000 °C to enable atomic or molecular species with sufficient volatility and chemical compatibility to diffuse through the target material and then effuse via a transfer line to an ion source for ionization. The target and ion source are held at a bias between 30 keV and 60 keV, enabling the electric field resulting from a grounded extraction electrode located ≈60 mm from the exit of the ion source to extract the ions as an "ion beam". The ion beam is directed through one of the ISOLDE dipole magnet mass separators, which separate the constituents according to momentum/charge (mv/q), and then transported to an experimental setup.

Laser light from the RILIS is directed a distance of ≈20 m to overlap with the effusing reaction products in a laser-atom interaction region, most commonly a tubular refractory metal "hot cavity" surface ion source [7,8]. ISOLDE surface ion sources have an inner diameter of 3 mm, a length of 34 mm and are resistively heated to ≈2000 °C. When operated without the RILIS laser light, surface ion sources rely on ionization on the walls of hot cavity [9]. They are applied for elements with sufficiently low ionization potentials, typically below 6 eV. Resistive heating of the hot cavity is still required during RILIS operation in order to reduce wall sticking times and enable the "hot cavity effect" [2,9], whereby thermal electron emission from the cavity walls enhances ion survival and extraction from the hot cavity. Therefore, despite the element selective ionization of the RILIS process, isobaric contamination that is surface ionized on the hot cavity walls can be problematic for certain experiments.

1.2. Motivation for this work

The application of the ISOLDE RILIS was requested to enhance the yield of radium isotopes for an experiment [10] on the Collinear Resonance Ionization Spectroscopy (CRIS) beam line at ISOLDE [11]. Radium is typically ionized at ISOL facilities by surface ion sources. The motivation for the development of an ionization scheme applicable at the ISOLDE RILIS was fivefold however:

- **The enhancement of the surface ionized fraction.** The surface ionization efficiency of radium in a 2000 °C tantalum hot cavity at ISOLDE does not approach unity. Consequently, the application of the RILIS has the potential to provide a valuable enhancement of the ionized fraction.
- **Signal identification.** By blocking or detuning the laser targeting the first resonant transition, it is typically possible to prevent the element specific RILIS enhancement, while effectively maintaining the experimental conditions for all other elements effusing through the hot cavity (most usefully isobaric contamination).
- **Compatibility with surface ion suppression techniques.** The hot cavity is not the only laser-atom interaction region utilized at ISOLDE. The Laser Ion Source and Trap (LIST) [12,13] has been demonstrated to suppress the surface ionized reaction products with a repeller located at the exit of the hot cavity and the RILIS being applied to ionize atomic reaction products in an ion guide downstream of the repeller. A RILIS ionization scheme for radium would therefore enable this method to be applied should an increase in the purity of radium ion beams be required.
- **Nuclear structure investigations.** In addition to its application as an ion source for element selective ion beam production, the ISOLDE RILIS is regularly used for in-source RIS [14], to investigate the ground state properties of nuclei (mean square charge radius, nuclear spin, magnetic dipole and electric quadrupole moments) [15]. The RILIS is applicable for such investigations in the heavier region of the nuclear chart, therefore radium would be well suited to such in-source RIS experiments.
- **Medical isotope production.** Radium isotopes have a long history of use for medical applications [16] which continues to the present day. ^{223}Ra is used to treat castration-resistant prostate cancers with metastases [17,18] and there is current interest in using ^{225}Ra as a generator for ^{225}Ac, which is considered to be particularly promising for medical applications [19]. Radium isotope collections have been undertaken at ISOL facilities as a result of this interest [20]. Dedicated facilities, applying ISOL principles for medical isotope production, are currently under development [21,22]. The application of a RILIS in such cases offers the possibility for increasing both the purity and the efficiency of collections.

2. Radium ionization at ISOL facilities

2.1. Surface ionization

The efficiency of surface ionization in the hot cavity environment has been discussed in detail in [9,23,24]. The ionization potential is a good guide to the comparative susceptibility of an element to surface ionization, however, the excited states of the atom and ion must also be considered [26]. This leads to an effective ionization potential (IP_{ef}) which can be calculated as

$$Q_x = \sum_j g_j \exp(-E_j/kT), \tag{1}$$

$$IP_{ef} = IP - kT \ln(Q_i/Q_a), \tag{2}$$

where Q_x is a partition function accounting for the influence of the ground or excited states j of the atom ($x = a$) or the ion ($x = i$), g is the degeneracy of the atomic or ionic state, E_j is the excitation energy of a particular state, k is the Boltzmann constant and T is the temperature. In the case of radium, IP_{ef} = 5.14 eV at 2060 °C.

Based on the equations and ion survival probability in a tungsten hot cavity discussed in [25], the surface ionization efficiency of radium in a tantalum hot cavity (work function ϕ = 4.25 eV [27]) can be estimated to be 5 %. This could be considered to be a conservative estimate due to the increased electron emission from tantalum compared to tungsten, however, given the number of uncertainties such an approach is justified. Efficiencies of surface ionized radium calculated from ISOLDE yields [28] support the feasibility of the estimation.

2.2. RILIS ionization

Based on the Boltzmann equation, 99.7 % of radium atoms are in the ground state at 2060 °C, hence all of the ionization schemes investigated originated from the $7s^2\ ^1S_0$ atomic ground state. The application of a RILIS for the ionization of radium was previously demonstrated at the TRIUMF-ISAC Facility [29], applying a $\{\lambda_1|\lambda_2|\lambda_3\}$ = {483 nm|818 nm|532 nm} ionization scheme with a non-resonant final excitation step [30]. A factor of three increase of the surface ionized signal was reported when applying the ionization scheme to ionize radium extracted from a pre-irradiated target heated to ≈1000 °C

For this study, literature data [5] was used to identify the first two transitions of an alternative ionization scheme better suited for use at the ISOLDE RILIS due to the avoidance of the 483 nm first step (that requires the operation of a Ti:Sa laser beyond its typical operational range or a UV pumped dye laser). This alternative ionization scheme employs a 714 nm first step and a 784 nm second step, exciting to the $7s8s\ ^3S_1$ state at 26 754 cm^{-1}, which is ≈15 819 cm^{-1} (≈632 nm) from the ionization potential at 42 573.36 (2) cm^{-1} [31]. Further information on these transitions is presented in Table 1.

Excitation to a state within the energy of a ≈632 nm photon from the ionization potential, enabled fundamental light from the RILIS dye lasers to be used as a final excitation step to probe the ionization continuum for autoionizing states.

Table 1
The resonant transitions investigated during the radium ionization scheme development originating from the $7s^2\ ^1S_0$ atomic ground state. Spectroscopic information on known lines is taken from [5].

Transition (cm^{-1})	Upper state	Term	J	Transition air wavelength (nm)	Enhancement factor	FWHM (cm^{-1})
0–13 999.36	7s7p	$^3P^o$	1	714.12167 (5)	–	0.46 (1)
13 999.36–26 754.01	7s8s	^3S	1	783.812 (2)	–	0.70 (2)
26 754.05–44 686 (4)	New AIS		0,1,2	557.51 (13)	3.3	62 (0.7)
26 754.05–43 951 (6)	New AIS		0,1,2	581.34 (21)	1.1	90 (1)
16 688.54[a] - 32 941.13	$7p^2$	^3P	2	615.119 (5)	–	2.28 (3)[b]
32 941.13–49 193.7	ECE[c]	–	–	615.119 (5)	3.8	–

Air wavelengths of the transitions to autoionizing states (AIS) are calculated using the equation of [35]. No attempt was made to deconvolve the 5–12 GHz linewidths of the scanning lasers from the FWHM. The uncertainties of the 558 nm and 581 nm transitions are dominated by the widths of the autoionizing resonances.
[a] The first 615 nm transition originates from the $7s7p\ ^3P_2$ level.
[b] The 615 nm light is understood to drive two atomic transitions, this may influence the observed FWHM of the observed resonance.
[c] Based on the observations summarized in Section 4.4, the 615 nm transition from $7p^{2\,3}P_2$ has an enhanced cross-section for atomic excitation (ECE).

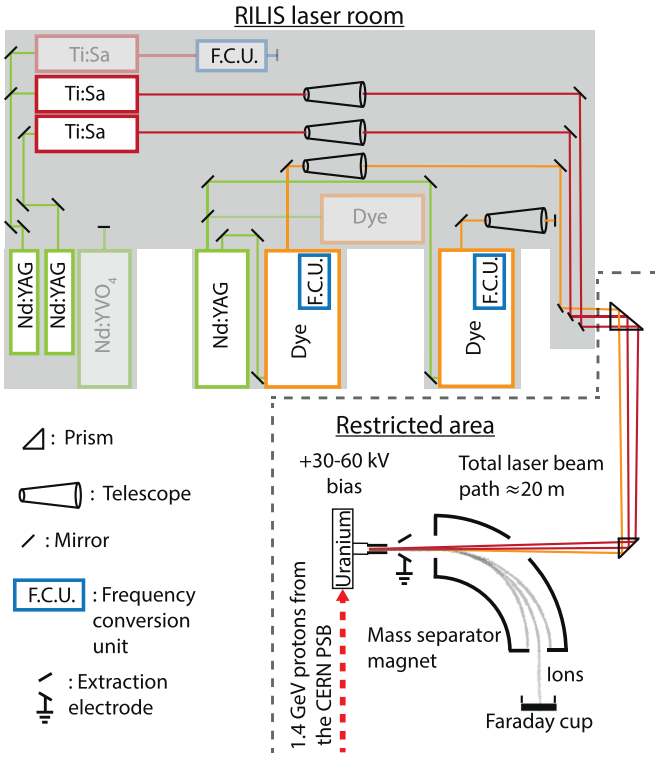

Fig. 1. A schematic of the experimental setup, the lasers used for this experiment are highlighted. A detailed discussion of the experimental setup is included in the text.

3. Experimental setup

The ISOLDE RILIS is depicted in Fig. 1. A system of three dye lasers and three Titanium:Sapphire (Ti:Sa) lasers are used in combination with 2ω, 3ω and 4ω harmonic generation to produce laser light with wavelengths spanning between 210 nm and 950 nm for multi-step resonance ionization. The lasers are typically pumped with 532 nm light from frequency-doubled Nd:YAG lasers. The dye lasers are pumped with 355 nm light, produced by frequency tripling the light from a Nd:YAG laser, for ionization schemes that require wavelengths in the region of 475 nm–540 nm. Where possible the use of UV pumped laser dyes is avoided due to the rate of degradation. The lasers are pulsed at a rate of 10 kHz, which is the optimal value based on currently achievable average and peak laser power and duty cycle considerations (the average mean residency time of an atom inside a hot cavity ion source is approximately 100 μs). The laser pulses delivered to the hot cavity are typically between 5 ns and 50 ns in duration depending on the laser and are typically overlapped by using a master clock to synchronize the output of the pump lasers. The laser light is stabilized in both position and wavelength, a more detailed description of the RILIS laser system can be found in [3].

The lasers used in the ionization scheme development reported here are highlighted in Fig. 1. Two Ti:Sa lasers were used to produce the light for the first and second excitation steps. Dye lasers operated with ethanol solutions of either Fluorescein 27, Rhodamine 6G or DCM dyes were scanned to search for autoionizing resonances, accessed via ionization schemes of {714 nm|784 nm|545 nm - 632 $nm^{dye\ scan}$}.

The laser light was focused using optics within the RILIS laser room and directed to converge inside a tantalum hot cavity surface ion source coupled to a UC_x target. Based on off-line calibration, the target and tantalum hot cavity were maintained at 1950 °C and 2060 °C respectively throughout these measurements. In the case of radium, since no stable isotope exists, the atoms were produced on-line at ISOLDE.

During the scans of the final excitation step, the wavelength of the laser light was measured using a HighFinesse/Ångstrom WS7 wavelength meter while the ion current on mass A = 226 was measured using a Faraday cup inserted downstream of the mass separator magnet, as depicted in Fig. 1.

4. Results and discussion

4.1. The search for autoionizing states

Following two-step {714 nm|784 nm} resonance excitation to the $7s8s\ ^3S_1$ state, dye lasers were used to scan the excitation energy band from the ionization potential to 45 094 cm^{-1} (632 nm to 545 nm). Ionization in this case was achieved via {714 nm|784 nm|545 nm - 632 $nm^{dye\ scan}$}. Three resonances were observed at wavelengths of 558 nm, 581 nm and 615 nm, additional details of the transitions are given in Table 1. The peaks in the spectra were fitted using either Voigt, Breit-Wigner-Fano or Inverse Polynomial peak functions. The different line shapes were the result of differing relative contributions from the spectral laser line shape, Doppler broadening of the atomic line, saturation effects and for the observed autoionizing states, asymmetric Fano Profiles. The scans of these resonances are presented in Fig. 2. The two resonances observable on the higher energy tail of the 558 nm autoionizing resonance in Fig. 2, match the 17 994.05 cm^{-1} and the 18 001.44 cm^{-1} transitions from $7s7p\ ^3P_1$ to $7s7d\ ^3D_2$ and $7s7d\ ^3D_1$ respectively. The uncertainty in the centroid positions of the autoionizing states at 558 nm and 581 nm are dominated by the FWHM of the resonances and the associated possibility for variations in the laser power over the range of the scan due to wavelength dependent dye efficiencies.

All three of the resonances were initially identified as autoionizing states, with full width at half maxima (FWHM) of 62 (0.7) cm^{-1}, 90 (1) cm^{-1} and 2.28 (3) cm^{-1} respectively (no attempt was made to deconvolve the ≈12 GHz linewidth of the dye lasers or account for

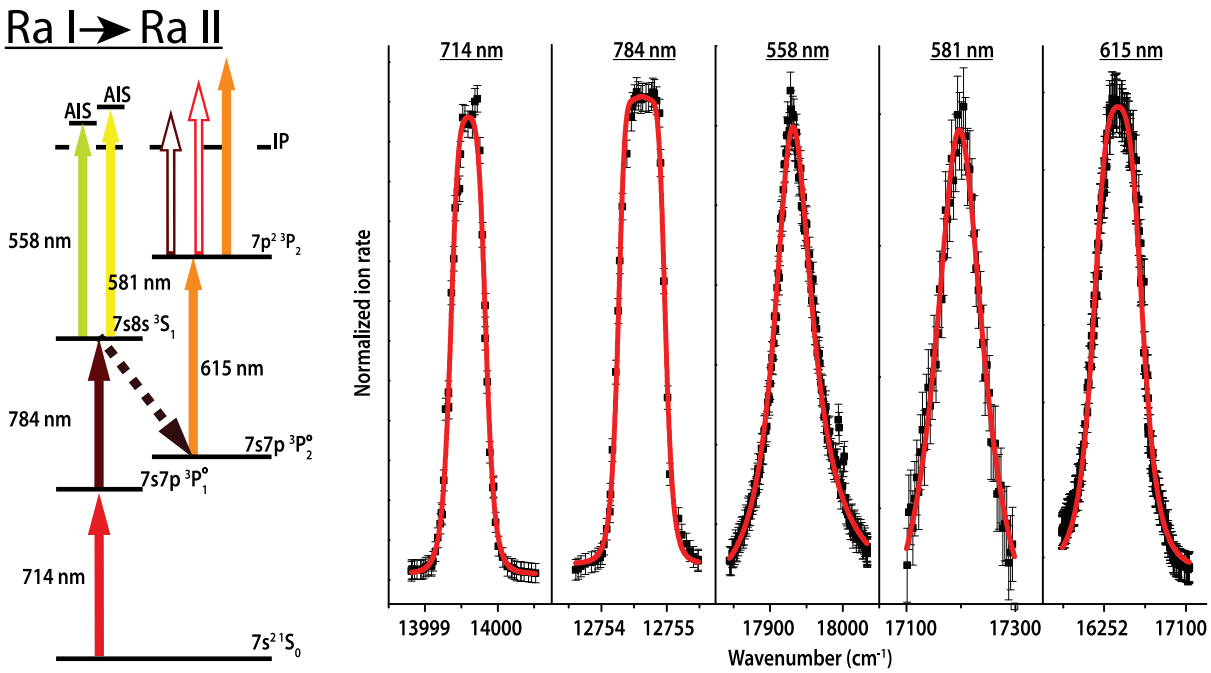

Fig. 2. The ionization schemes investigated during the radium ionization scheme development and scans of the resonances. Levels labeled AIS are identified to be autoionizing states, the dashed line labeled IP represents the first ionization potential of atomic radium. Based on the observations summarized in Section 4.4, 615 nm light is the dominant ionization step for electrons populating the $7p^{23}P_2$ excited state. This is reflected by the solid arrow for a 615 nm excitation step from $7p^{23}P_2$. The error bars on the data points of the resonance scans are estimated based on the precision of the Faraday cup used to measure the ion current.

power broadening). Autoionizing resonances with both comparable and greater FWHM have been observed for other elements such as the alkaline earth metal homologue barium [32]. However, an unexpected insensitivity to blocking either of the first two steps was observed when the {714 nm|784 nm|615 nm} ionization scheme was tested at the CRIS beamline [11], where a charge exchange cell is used to neutralize ions before re-ionization. Following an additional review of the literature, it was realized that the 615 nm line was a known transition from the 7s7p $^3P_2$ metastable state. On the CRIS beamline, the metastable state is understood to have been populated during the charge exchange process [33], while during hot cavity RILIS operation it could only be significantly populated via a decay from the 7s8s $^3S_1$ state, as from the Boltzmann equation the thermal population of the 7s7p $^3P_2$ state at 2060 °C is just 0.02 %. This is the first time optical pumping has been observed in hot cavity RILIS operation. Similar non-laser driven transitions within resonance ionization schemes have been observed in other laser-atom interaction environments [34], where the intermediate non-laser driven stage was reported to be resulting from interactions with a buffer gas.

Excitation from 7s7p $^3P_2$ to $7p^{23}P_2$ with 615 nm light results in an excited state ≈9632 cm^{-1} below the ionization potential. Thus it was unexpected that applying the {714 nm|784 nm|558 nm} ionization scheme (ionizing via an autoionizing state) and applying the {714 nm|784 nm|993 nm^{decay}|615 nm, 714 nm, 784 nm} ionization scheme (which relies on photons with energies matching preceding transitions for the final ionizing transition) yielded a similar factor of 3–4 increase in the ion rate. Due to time constraints, further investigations were limited to these two ionization schemes corresponding to the highest ionization efficiency. The sensitivity to the timing overlap of the pulsed laser light and the saturation of the transitions were investigated to clarify the situation.

4.2. Timing scans

In order to demonstrate optical pumping within the hot cavity environment, the 615 nm laser pulses were delayed with respect to the temporally overlapped 714 nm and 784 nm pulses while monitoring the ion current on the Faraday cup inserted downstream of the dipole mass separator. The variation in ion current with the time delay of the 615 nm laser pulses is presented in Fig. 3, together with the results of delaying the 558 nm transition in the same manner for comparison.

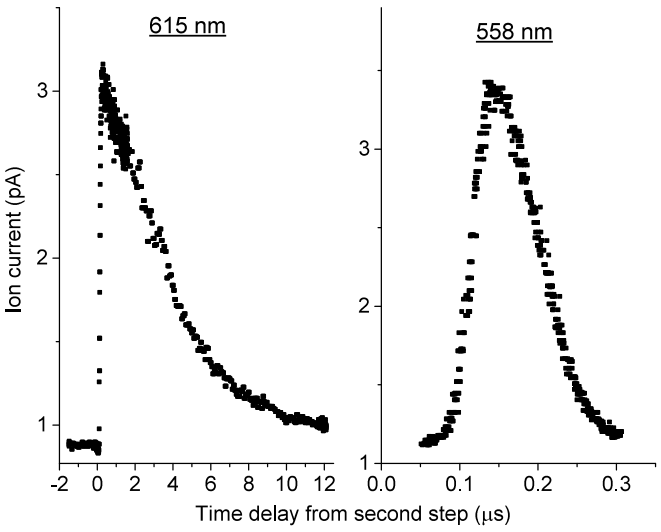

Fig. 3. The change in ion current with a variation in the synchronization of the second and third step transitions. An off-set of ≈100 ns with respect to the timing of the second step transition is the result of the laser pulse timing being measured at different locations. Further details are discussed in the text.

The comparative insensitivity of the {714 nm|784 nm|993 nm^{decay}|615 nm, 714 nm, 784 nm} ionization scheme to the timing overlap of the final step with the first two transitions, can be understood as resulting from the decay from the 7s8s $^3S_1$ state to the 7s7p $^3P_2$ state, from which there is no allowed transition path to the $7s^{21}S_0$ atomic

ground state. However, the comparatively small reduction in ionization efficiency when delaying the 615 nm transition from the first two excitation steps by 1 μs also indicates that the 615 nm transition is the dominant ionization step from the $7p^{23}P_2$ excited state. Thus the ionization scheme can be considered to be {714 nm|784 nm|993 nm^{decay}|615 nm|615 nm}.

4.3. Saturation measurements

Saturating the transitions of an ionization scheme maximizes its efficiency and reduces the impact of any potential deterioration in laser power over the course of an experiment. Saturation measurements of the 714 nm, 784 nm, 558 nm and 615 nm transitions were made by varying the laser power of each transition individually, while monitoring the ion current. The results are presented in Fig. 3. The variation in the error bars on specific measurement points is the result of the measurements taking place at different times, with differing ion currents.

The saturation measurements presented in Fig. 3 were fitted using Eq. 3, a commonly used function [36,37] which relates the ion current to the laser power delivered for each resonant transition

$$I = B + M(P/P_{1/2sat})/(P/(P_{1/2sat} + 1)), \quad (3)$$

where I is the ion current, B is the background ion current when the transition is blocked, M is the maximum ion current achievable with a fully saturated transition, P is the laser power delivered to the laser-atom interaction region and $P_{1/2sat}$ is the laser power required to achieve 50 % of M. The equation assumes the dominant contribution to the ionization process is from resonant excitation.

The uncertainties in the $P_{1/2sat}$ values are dominated by the uncertainty in the transmission of the laser light to the hot cavity. The transmission efficiency is assumed to be constant during the saturation measurement therefore it was not included as an uncertainty on each measurement point but rather in the error in the value for $P_{1/2sat}$, with a transmission efficiency of between 40 and 60 % considered. The plots shown in Fig. 3 assume a 50 % transmission efficiency.

The 714 nm, 784 nm and 615 nm transitions were demonstrated to be deeply saturated with the available laser power; while the 558 nm transition was found to be on the edge of saturation reaching approximately 0.78 M with an estimated 2.8 W of laser light delivered to the ion source. By extrapolating from the saturation fit, doubling the laser power delivered to the laser-atom interaction region would increase the saturation level to 0.87 M. Based on the saturation measurements, it is clear that the {714 nm|784 nm|993 nm^{decay}|615 nm|615 nm} ionization scheme offers the greatest operational stability for on-line radioactive ion beam production.

The significant population of the $7s7p\ ^3P_2$ state, highlights the potential limitation to some RILIS ionization scheme efficiencies due to the decay of excited states within the time frame of the applied ionization scheme. For a given pulse length, such losses would make it additionally challenging to saturate a transition.

4.4. An enhanced cross-section for excitation from $7p^{23}P_2$ to 49 193.7 cm^{-1}

The timing synchronization scans presented in Fig. 3 demonstrate that the 615 nm transition (exciting from the $7p^{23}P_2$ state to 49 193.7 cm^{-1}) was the dominant ionization step, despite there being a comparable number of 714 nm and 784 nm photons (capable of exciting from the $7p^{23}P_2$ state to 46 940.5 cm^{-1} and 45 695.8 cm^{-1} respectively). This suggests a significantly increased cross-section for excitation from $7p^{23}P_2$ to 49 193.7 cm^{-1} compared to either 46 940.5 cm^{-1} or 45 695.8 cm^{-1}. Given that the 615 nm transition is the dominant ionization step, the inference of an enhanced cross-section for excitation to 49 193.7 cm^{-1} is supported by the deep saturation of the influence of 615 nm photons presented in Fig. 4. By comparison, non-resonant final step transitions in RILIS ionization schemes using a dedicated 532 nm frequency-doubled Nd:YVO_4 Blaze laser [14] are not typically saturated

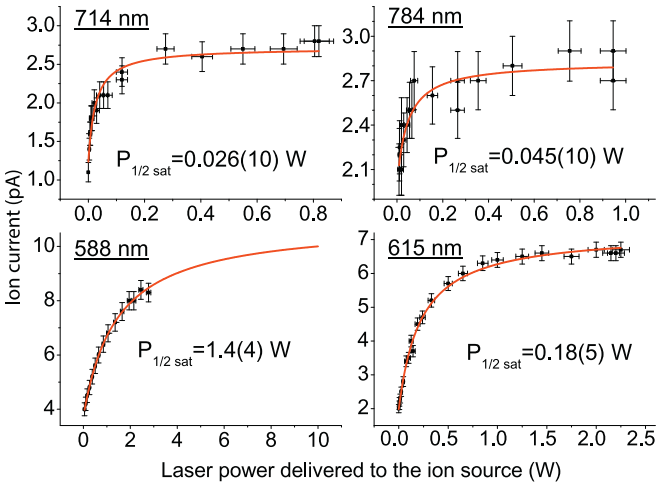

Fig. 4. Saturation measurements plotting the laser power delivered to the hot cavity ion source against the radium ion current for four of the investigated transitions. The uncertainty on individual measurement points is related to the precision of the measurement devices and the method of recording. An additional uncertainty is included for the $P_{1/2sat}$ values, considering a transmission efficiency of the laser light to the ion source between 40 and 60 %.

despite delivering an estimated 24 W of laser light to the laser-atom interaction region. Applying a fourth laser, as part of a {714 nm|784 nm|993 nm^{decay}|615 nm|605 − 625 nm} ionization scheme, could clarify whether the efficiency of the {714 nm|784 nm|993 nm^{decay}|615 nm|615 nm} ionization scheme is the result of an autoionizing state in the vicinity of 49 193.7 cm^{-1}.

4.5. On-line application

Following the ionization scheme development reported here, RILIS ionization of atomic radium has been successfully applied on two occasions to produce radioactive ion beams for experiments on the CRIS beam line [10]. Based on the enhancement and the degree of saturation, the {714 nm|784 nm|993 nm^{decay}|615 nm|615 nm} ionization scheme was identified as optimal for on-line RILIS operation.

For future on-line operation, the application of a fourth laser producing 558 nm light to additionally target radium atoms in the $7s8s\ ^3S_1$ excited state, may result in an enhanced overall efficiency. This would correspond to the simultaneous application of ionization schemes of {714 nm|784 nm|993 nm^{decay}|615 nm|615 nm} and {714 nm|784 nm|558 nm}. A similar approach is commonly applied for the ionization of elements such as indium, aluminium and gallium at the ISOLDE RILIS, where there is a significant percentage of the atomic population existing in a low lying thermally populated atomic level (at ≈2000 °C) [3].

The ionization schemes presented here include excitations via s→p transitions, which exhibit the necessary sensitivity to nuclear structure effects for future in-source resonance ionization spectroscopy experiments. The applicability of the 714 nm line for such investigations has already been demonstrated [38].

5. Conclusion

Three ionization schemes for atomic radium were developed. Autoionizing states of atomic radium were observed for the first time, found to be at 43 951 (6) cm^{-1} and 44 686 (4) cm^{-1} and accessed via ionization schemes of {714 nm|784 nm|581 nm} and {714 nm|784 nm|558 nm} respectively. The optimal ionization scheme of {714 nm|784 nm|993 nm^{decay}|615 nm|615 nm} was found to provide an enhancement factor of 3.8 with respect to surface ionization in a tantalum hot cavity heated to 2060 °C. This ionization

scheme includes five atomic transitions in the process of exciting to 49 193.7 cm^{-1}. It is the first time that optical pumping has been employed in a hot cavity RILIS ionization scheme. All of the laser driven excitation steps were found to be deeply saturated, suggesting an enhanced cross-section for atomic excitation from the $7p^{23}P_2$ excited state to 49 193.7 cm^{-1}.

Following this ionization scheme development, RILIS ionization has been successfully applied on two occasions to increase the yield of exotic radium isotopes for experiments on the CRIS beam line at ISOLDE. In addition to offering the possibility of increasing the yield of radium ion beams, the new ionization schemes enable the possibility for signal identification and the future application of surface ion suppression techniques. The first (714 nm) excitation step, common to all of the ionization schemes, is sufficiently sensitive to nuclear structure effects to enable future in-source resonance ionization spectroscopy experiments at the ISOLDE RILIS.

Acknowledgements

This project has received funding through the European Union's Seventh Framework Programme for Research and Technological Development under Grant Agreements 262010 (ENSAR), 267194 (COFUND), and 289191 (LA^3NET). This work was supported by the ERC Consolidator Grant No. 648381; the IUAP-Belgian State Science Policy (BRIX network P7/12), FWO-Vlaanderen (Belgium) and GOAs 10/010 and 10/05 and starting grant STG 15/031 from KU Leuven; the Science and Technology Facilities Council Consolidated Grant No. ST/F012071/1, Continuation Grant No. ST/J000159/1 and Ernest Rutherford Grant No. ST/L002868/1; and the European Unions Horizon 2020 Framework through ENSAR2 No. 654002. We acknowledge the financial aid from the Ed Schneiderman Fund at New York University.

References

[1] M.J.G. Borge, K. Blaum, Focus on Exotic Beams at ISOLDE: a Laboratory portrait, J. Phys. 45 (1) (2018) 010301.
[2] V.I. Mishin, V.N. Fedoseyev, H.-J. Kluge, V.S. Letokhov, H.L. Ravn, F. Scheerer, Y. Shirakabe, S. Sundell, O. Tengblad, Chemically selective laser ion-source for the CERN-ISOLDE on-line mass separator facility, Nucl. Instrum. Methods Phys. Res., Sect. B 73 (4) (1993) 550–560.
[3] V. Fedosseev, K. Chrysalidis, T. Day Goodacre, B. Marsh, S. Rothe, C. Seiffert, K. Wendt, Ion beam production and study of radioactive isotopes with the laser ion source at ISOLDE, J. Phys. 44 (8) (2017) 084006.
[4] V.S. Letokhov, Laser Photoionization Spectroscopy, 1 edition, ACADEMIC PRESS INC, London, 1987.
[5] U. Dammalapati, K. Jungmann, L. Willmann, Compilation of Spectroscopic Data of Radium (Ra I and Ra II), J. Phys. Chem. Ref. Data 45 (1) (2016) 013101.
[6] O. Kofoed-Hansen, K.O. Nielsen, Short-Lived Krypton Isotopes and their Daughter Substances, Phys. Rev. 82 (1) (1951) 96–97.
[7] G.J. Beyer, E. Herrmann, A. Piotrowski, V.J. Raiko, H. Tyrroff, A new method for rare-earth isotope separation, Nucl. Inst. Methods 96 (3) (1971) 437–439.
[8] P.G. Johnson, A. Bolson, C.M. Henderson, A high temperature ion source for isotope separators, Nucl. Inst. Methods 106 (1) (1973) 83–87.
[9] R. Kirchner, On the thermoionization in hot cavities, Nucl. Instrum. Methods Phys. Res. Sect. A 292 (2) (1990) 203–208.
[10] K.M. Lynch, S.G. Wilkins, J. Billowes, C.L. Binnersley, M.L. Bissell, K. Chrysalidis, T.E. Cocolios, T. Day Goodacre, R.P. de Groote, G.J. Farooq-Smith, D.V. Fedorov, V.N. Fedosseev, K.T. Flanagan, S. Franchoo, R.F. Garcia Ruiz, W. Gins, R. Heinke, Á. Koszorús, B.A. Marsh, P.L. Molkanov, P. Naubereit, G. Neyens, C.M. Ricketts, S. Rothe, C. Seiffert, M.D. Seliverstov, H.H. Stroke, D. Studer, A.R. Vernon, K.D.A. Wendt, X.F. Yang, Laser-spectroscopy studies of the nuclear structure of neutron-rich radium, Phys. Rev. C 97 (2) (2018) 024309.
[11] T.E. Cocolios, H.H. Al Suradi, J. Billowes, I. Budinčević, R.P. de Groote, S. De Schepper, V.N. Fedosseev, K.T. Flanagan, S. Franchoo, R.F. Garcia Ruiz, H. Heylen, F. Le Blanc, K.M. Lynch, B.A. Marsh, P.J.R. Mason, G. Neyens, J. Papuga, T.J. Procter, M.M. Rajabali, R.E. Rossel, S. Rothe, G.S. Simpson, A.J. Smith, I. Strashnov, H.H. Stroke, D. Verney, P.M. Walker, K.D.A. Wendt, R.T. Wood, The Collinear Resonance Ionization Spectroscopy (CRIS) Experimental Setup at CERN-ISOLDE, Nucl. Instrum. Methods Phys. Res. Sect B 317 (2013) 565–569.
[12] K. Blaum, C. Geppert, H.-J. Kluge, M. Mukherjee, S. Schwarz, K. Wendt, A novel scheme for a highly selective laser ion source, Nucl. Instrum. Methods Phys. Res., Sect. B 204 (2003) 331–335.
[13] D.A. Fink, S.D. Richter, B. Bastin, K. Blaum, R. Catherall, T.E. Cocolios, D.V. Fedorov, V.N. Fedosseev, K.T. Flanagan, L. Ghys, A. Gottberg, N. Imai, T. Kron, N. Lecesne, K.M. Lynch, B.A. Marsh, T.M. Mendonca, D. Pauwels, E. Rapisarda, J.P. Ramos, R.E. Rossel, S. Rothe, M.D. Seliverstov, M. Sjödin, T. Stora, C. Van Beveren, K.D.A. Wendt, First application of the Laser Ion Source and Trap (LIST) for on-line experiments at ISOLDE, Nucl. Instrum. Methods Phys. Res., Sect. B (2013).
[14] B. Marsh, T. Day Goodacre, D. Fink, S. Rothe, M. Seliverstov, N. Imai, M. Sjodin, R. Rossel, Suitability Test of a High Beam Quality Nd:YVO4 Industrial Laser for the ISOLDE RILIS Installation, Technical Report, CERN, Geneva, 2013.
[15] P. Campbell, I.D. Moore, M.R. Pearson, Laser spectroscopy for nuclear structure physics, Prog. Part. Nucl. Phys. 86 (2016) 127–180.
[16] J.M.H. MacLeod, Further observations on the Therapeutic Value of Radium and Thorium, BMJ 1 (2267) (1904) 1366–1369.
[17] C. Parker, S. Nilsson, D. Heinrich, S.I. Helle, J.M. O'Sullivan, S.D. Fosså, A. Chodacki, P. Wiechno, J. Logue, M. Seke, A. Widmark, D.C. Johannessen, P. Hoskin, D. Bottomley, N.D. James, A. Solberg, I. Syndikus, J. Kliment, S. Wedel, S. Boehmer, M. Dall'Oglio, L. Franzén, R. Coleman, N.J. Vogelzang, C.G. O'Bryan-Tear, K. Staudacher, J. Garcia-Vargas, M. Shan, Ø.S. Bruland, O. Sartor, Alpha Emitter Radium-223 and Survival in Metastatic Prostate Cancer, N. Engl. J. Med. 369 (3) (2013) 213–223.
[18] R.C.D. Bolton, G. Francesco, Bone radionuclide therapy and increased survival with radium-223 is the way to go for nuclear medicine: the offer that oncologists cannot refuse, Eur. J. Nucl. Med. Mol. Imaging 45 (5) (2018) 822–823.
[19] C. Kratochwil, F. Bruchertseifer, H. Rathke, M. Bronzel, C. Apostolidis, W. Weichert, U. Haberkorn, F.L. Giesel, A. Morgenstern, Targeted -therapy of metastatic castration-resistant prostate cancer with 225 Ac-PSMA-617: Dosimetry estimate and empiric dose finding, J. Nuclear Med. 58 (10) (2017) 1624–1631.
[20] C. Hoehr, F. Bénard, K. Buckley, J. Crawford, A. Gottberg, V. Hanemaayer, P. Kunz, K. Ladouceur, V. Radchenko, C. Ramogida, A. Robertson, T. Ruth, N. Zacchia, S. Zeisler, P. Schaffer, Medical isotope production at TRIUMF from imaging to treatment, Phys. Proc. 90 (2017) 200–208.
[21] V.N. Panteleev, A.E. Barzakh, L.Kh. Batist, D.V. Fedorov, V.S. Ivanov, F.V. Moroz, P.L. Molkanov, S.Yu. Orlov, Yu.M. Volkov, The radioisotope complex project at the Petersburg Nuclear Physics Institute, Rev. Sci. Instr. 86 (12) (2015) 123510.
[22] R. dos Santos Augusto, L. Buehler, Z. Lawson, S. Marzari, M. Stachura, T. StoraCERN-MEDICIS Collaboration, CERN-MEDICIS (Medical Isotopes Collected from ISOLDE): A New Facility, Appl. Sci. 4 (2) (2014) 265–281.
[23] D.M. Wayne, W. Hang, D.K. McDaniel, R.E. Fields, E. Rios, V. Majidi, The thermal ionization cavity (TIC) source: elucidation of possible mechanisms for enhanced ionization efficiency, Int. J. Mass Spectrom. 216 (1) (2002) 41–57.
[24] M. Turek, Ionization of short-lived isotopes in a hot cavity â€ Numerical simulations, Vacuum 104 (2014) 1–12.
[25] T. Day Goodacre, K. Chrysalidis, D.V. Fedorov, V.N. Fedosseev, B.A. Marsh, P.L. Molkanov, R.E. Rossel, S. Rothe, C. Seiffert, The identification of autoionizing states of atomic chromium for the resonance ionization laser ion source of the ISOLDE radioactive ion beam facility, Spectrochim. Acta Part B 129 (2017) 58–63.
[26] É.Y. Zandberg, N.I. Ionov, Surface ionization, Soviet Phys. Uspekhi 2 (2) (1959) 255–281.
[27] CRC, Physical constants of organic compounds, CRC Handbook of Chemistry and Physics, CRC Press/Taylor & Francis, Boca Raton, FL, 2017.
[28] S. Lukić, F. Gevaert, A. Kelić, M.V. Ricciardi, K.H. Schmidt, O. Yordanov, Systematic comparison of ISOLDE-SC yields with calculated in-target production rates, Nucl. Instru. Methods Phys. Res. Sect. A 565 (2) (2006) 784–800.
[29] J. Dilling, R. Krücken, G. Ball, ISAC overview, Hyperfine Interactions 225 (1–3) (2014) 1–8.
[30] S. Raeder, J. Lassen, H. Heggen, A. Teigelhöfer, In-source spectroscopy on astatine and radium for resonant laser ionization, Hyperfine Interactions 227 (1–3) (2014) 77–83.
[31] J.A. Armstrong, J.J. Wynne, F.S. Tomkins, Bound, 7snp 1P1 0 series in Ra I: measurements and predictions, J. Phys. B 13 (5) (1980) L133–L137.
[32] M.A. Kalyar, M. Rafiq, M.A. Baig, Interaction of the 6p2 1S0 broad resonance with 5dnd J = 0 autoionizing resonances in barium, Phys. Rev. A 80 (5) (2009) 052505.
[33] S.G. Wilkins, Collinear Resonance Ionization Spectroscopy of Exotic Francium and Radium Isotopes, PhD The University of Manchester, 2018.
[34] M. Laatiaoui, W. Lauth, H. Backe, M. Block, D. Ackermann, B. Cheal, P. Chhetri, C.E. Düllmann, P. van Duppen, J. Even, R. Ferrer, F. Giacoppo, S. Götz, F.P. Heßberger, M. Huyse, O. Kaleja, J. Khuyagbaatar, P. Kunz, F. Lautenschläger, A.K. Mistry, S. Raeder, E.M. Ramirez, T. Walther, C. Wraith, A. Yakushev, Atom-at-a-time laser resonance ionization spectroscopy of nobelium, Nature 538 (7626) (2016) 495–498.
[35] K.P. Birch, M.J. Downs, An Updated Edlén Equation for the Refractive Index of Air, Metrologia 30 (3) (1993) 155–162.
[36] S. Rothe, An All-Sstate Laser System for the Laser Ion Source RILIS and in-Source Laser Spectroscopy of Astatine at ISOLDE, Doctoral thesis J.G. University of Mainz, 2012.
[37] D.A. Fink, Improving the Selectivity of the ISOLDE Resonance Ionization Laser Ion Source and In-Source Laser Spectroscopy of Polonium, Doctoral thesis Heidelberg University, 2014.
[38] K. Wendt, S.A. Ahmad, W. Klempt, R. Neugart, E.W. Otten, H.H. Stroke, On the hyperfine structure and isotope shift of radium, Molecules and Clusters 4 (3) (1987) 227–241.